International Journal of Applied Pharmaceutics

ISSN- 0975-7058 Vol 18, Issue 3, 2026

Original Article

IN SILICO ANALYSIS OF NOVEL COMPOUNDS TARGETING THE SARS-COV-2 PAPAIN-LIKE PROTEASE

HABEEB RAJA S.[1], ANBUMURUGAN S. P.[1], IRFANA K.[2], SUSMITHA V.[1], ARUN KESAVH S.[1], NITHEESH A.[1], MUTHUKUMARAN M.[3], MOHD ABDUL BAQI[3*]

[1]Department of Pharmaceutical Chemistry, Arulmigu Kalasalingam College of Pharmacy, Kalasalingam Academy of Research and Education, Krishnan Koil, Tamil Nadu, India. [2]Velammal Medical College, Hospital and Research Institute, Velammal Village, Madurai, Tamil Nadu, India. [3]Department of Pharmaceutics, Sri Blaji Vidyapeeth School of Pharmacy, Karaikal, Pondicherry, India
[*]Corresponding author: Mohd Abdul Baqi; [*]Email: sufyan687@gmail.com

Received: 27 Dec 2025, Revised and Accepted: 23 Feb 2026

ABSTRACT

Objective: The present study aimed to design and computationally evaluate *pyrimidine-based* ring derivatives as potential inhibitors of *SARS-CoV-2* papain-like protease (PLpro).

Methods: To find the binding affinity between designed compounds and papain-like protease (PLpro) was used molecular docking. Binding free energy and complex stability were verified using molecular mechanics–generalized born surface area (MM-GBSA) simulations. Additionally, the QikProp tool was used to estimate the absorption, distribution, metabolism, and excretion (ADME) characteristics of substances.

Results: Docking analysis showed that compound 2 had a glide score of-5.31 kcal/mol, comparable to the *co-crystal* (-2.10 kcal/mol). Key interactions with Ile548, Ser549, Ala550, Arg836, Asp833 and Ser814 contributed to its stability. Binding free energy analysis revealed that compound 2 (-74.24 kcal/mol).

Conclusion: Compound 2 demonstrated potential interactions with papain-like protease (PLpro), comparable to the co-crystal. These findings suggest that compound 2 is a promising lead candidate for *SARS-CoV-2* (PLpro)-targeted therapy, warranting further preclinical and biological validation.

Keywords: Papain-like protease (PLpro) inhibitors, Molecular docking, MM-GBSA, ADME, *SARS-CoV-2*, Drug discovery

DOI: https://dx.doi.org/10.22159/ijap.2026v18i3.57936 Journal homepage: https://innovareacademics.in/journals/index.php/ijap

INTRODUCTION

At the end of 2019, for the first time, *SARS-CoV-2* was identified, which was the reason for *COVID-19*, which was dangerous for the world [1]. According to who this virus has caused over 6 million deaths. In each country, hundreds of people have been affected. Presently, vaccines and anti-viral drugs are available, but new variants of *SARS-CoV-2* are still coming to the market. Because of the limitations of available treatments, must prepare a new anti-viral drug [2]. *SARS-CoV-2* virus belongs to coronaviridiae family and this contains a big RNA genome. This gene is responsible for virus replication and escaping easily from our body's immune system because of its structure and the presence of proteins inside the virus, which give signals. In this virus, a very important protein is present, which is papain-like protease (PLpro). PLpro will break viral poly proteins; these viral poly proteins help in developing needy functional units for the virus [3]. It will not only do this act on *ubiquitin* but also remove *ubiquitin,* which is present on host cell protein which suppresses IIR response. Because of viral replication and immune suppression, PLpro is one of the most important targets. On PLpro, few scientists have done research using the drug that they have invented, which showed limited efficacy, and the remaining drugs are still under investigation [4]. Although several PLpro inhibitors have been reported, including the well-known lead compound GRL-0617, their further development has been limited by moderate potency, suboptimal pharmacokinetic properties, and poor oral bioavailability. In this context, the present study focuses on the design of *pyrimidine-based* scaffolds aimed at achieving improved drug-like properties, enhanced oral bioavailability, and a potentially favorable resistance profile compared to existing PLpro inhibitors. So, designing inhibitors that contain better binding affinity and improved pharmacological properties is essential. It can effectively inhibit PLpro, virus replication capacity and the ability of the virus to escape from the immune system can be suppressed to a great extent [5]. Because of this, the viral load in the patient is reduced, and there is also a chance of inhibiting disease severity. In this study, we will target *SARS-CoV-2* papain-like protease (PLpro) (PDB id 7D4F) using *in silico* approaches, including molecular docking and drug likeness prediction analysis. Despite the identification of PLpro as a promising antiviral target, no PLpro-directed drugs have yet advanced to clinical approval, and most reported inhibitors have stalled at early discovery or preclinical stages due to limitations related to binding efficiency, oral bioavailability and toxicity concerns. The novelty of the present study lies in the rational exploration of *pyrimidine-based* scaffolds as PLpro inhibitors, focusing on their binding interactions, predicted oral bioavailability, and safety profile. Compounds demonstrating favorable binding affinity, acceptable ADME properties, and low predicted toxicity are proposed as promising candidates for further chemical synthesis and subsequent *in vitro* biological evaluation, thereby providing a systematic pathway for advancing PLpro inhibitor development. This study reports a novel *pyrimidine-based* PLpro inhibitor featuring a *5-methyl-2,6-dioxo-pyrimidine* core linked to a *phenoxy-N-phenylacetamide* framework. Unlike reported PLpro inhibitors such as GRL0617 that rely on *peptidomimetic* or *naphthalene* scaffolds, the present design adopts a non-*peptidic*, drug-like architecture to enhance stability and binding adaptability. The *uracil-like pyrimidine* moiety offers improved hydrogen-bonding interactions with the PLpro active site, while the *phenoxy–acetamide* linker provides structural flexibility, representing a clear structural advancement over existing PLpro inhibitors.

MATERIALS AND METHODS

Preparation of ligands

The structures of ten different ligands (supplementary data 1) were processed using the ligPrep module in the maestro molecular modelling software, utilising the OPLS3 force field. Determining the appropriate protonation states of molecules under physiological conditions can be complex. To address this, the Epik module in the Maestro suite was employed to accurately predict the protonation states of strained molecules

based on text-mining analyses. Additionally, this module generated stereoisomers of the compounds at the physiological pH range (7.4±0.4). Understanding the protonation states of these molecules provides valuable insights into their interactions with proteins and other small molecules within biological systems.

Protein preparation

The protein data bank (PDB) provided the protein structural data that was needed for our investigation. The target protein that was chosen has 326 residues in total, and utilised the PDB ID: 7D4F structure that is associated with the target protein. Using the default parameters included in the maestro protein preparation module, was pre-processed the complete protein structure. The prime module in maestro was used to recreate the loops, atoms, and side chains that were absent from the protein backbone. Ramachandran plot generated by Schrodinger 2023-4 and analysis has shown that 99% of the total residues are in permitted locations. The stereochemical quality of the prepared (PL^{pro}) (PDB ID: 7D4F) structure was evaluated using the Ramachandran plot. The majority of amino acid residues were observed in the favored (red) and additionally allowed (yellow) regions, confirming correct backbone geometry and proper folding of the protein. Only a very small fraction of residues was located in the disallowed regions, which is within acceptable limits and does not significantly affect the overall protein stability. The distribution pattern indicates that the protein adopts a stable and energetically favorable conformation, thereby validating its suitability for molecular docking and further *in silico* studies [6, 7] as shown in fig. 1.

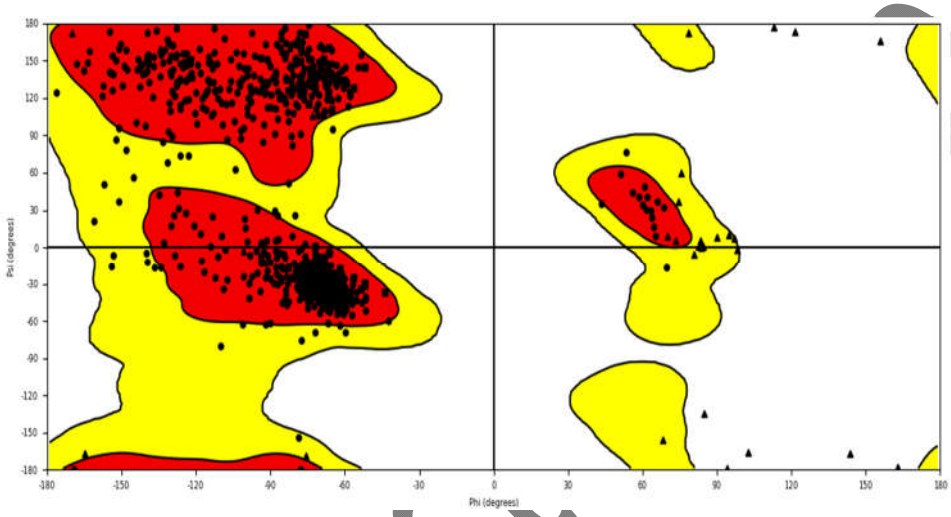

Fig. 1: Ramachandran plot of SARS-CoV-2 (PL^{pro}) (PDB ID: 7D4F) showing the distribution of φ and ψ torsion angles, confirming conformational stability of the prepared structure

This attests to the manufactured protein structure's dependability and structural quality. In addition, was estimated the impact of water molecules on the catalytic domain using molecular modelling. The generating a grid box centered on the co-crystallized ligand binding site. A cubic grid of 20 Å was constructed at the coordinates X =-34.12, Y = 18.32, Z = 46.76, encompassing the catalytically relevant region of the protein [8]. This grid served as the docking space for subsequent virtual screening studies. A visual representation of the defined docking grid is shown in fig. 2.

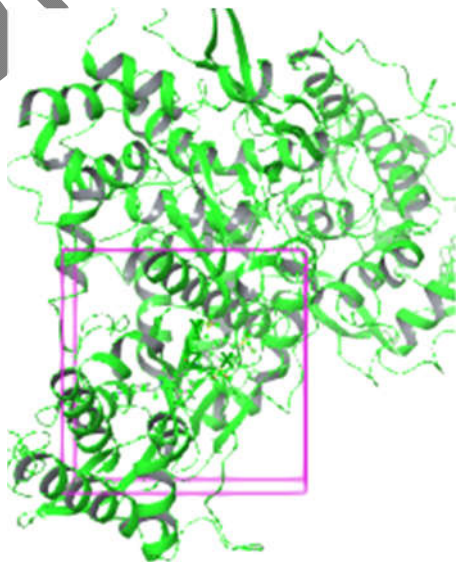

Fig. 2: Grid box generation for molecular docking at the catalytic active site of the papain-like protease (PLpro) of SARS-CoV-2 (PDB ID: 7D4F). The docking grid (20 Å × 20 Å × 20 Å) was centered on the catalytic triad residues, defining the active-site pocket used for docking calculations

Molecular docking

Molecular docking was conducted using the Schrödinger suite 2023-4, specifically the glide module in the (extra precision) (XP) mode, to predict ligand interactions within the catalytic site of the target protein. The selected molecules, along with the papain-like protease (PLpro) substrate, were docked using glide to generate poses with high docking scores. Glide's scoring function evaluates retrieved conformations to assign docking scores [9]. For each molecule, ten bioactive conformers were generated by placing sequences within the catalytic site of ten co-crystallized molecules. Docking simulations were carried out using the XP visualizer in the maestro molecular modeling suite, a grid-based docking program, to identify optimal binding poses in the papain-like protease (PLpro) catalytic site. Genetic algorithms and docking algorithms were utilized to refine and select the most suitable conformations based on top docking scores. The selected target protein (PDB ID: 7D4F) and the identified molecules were used as inputs for molecular docking. The XP visualiser program was utilised to analyse the docking results for molecular docking. The Glide module was used for all docking simulations, and XP mode was used throughout the whole procedure [10]. The scaling factor for target enzyme molecules was set at 0.8, and the partial atomic charge threshold was set at 0.15. The best docked complex was chosen after docking, taking into account the glide docking ratings. Finally, XP visualiser was utilised once more for the in-depth examination of the protein–ligand interactions found in the chosen docked configurations [11].

Binding free energy calculations using prime MM-GBSA

Using the Prime MM-GBSA method included in Schrödinger suite 2023-4, was determined the binding free energy of each protein-ligand combination. This method's capacity to incorporate various energy contributions allows us to evaluate binding affinity in a thorough manner [12]. Prim MM-GBSA will combine molecular mechanics energies with implicit solvation models to determine the binding free energy. This procedure involves several crucial phases. In order to minimise energy, was first employed the OPLS3e force field. This force field was specifically created to accurately simulate biomolecular interactions. The implicit solvation model VSGB 2.0 (variable dielectric generalised born) was used to take solvation effects into account [13]. This model will depict hydrophobic effects, self-contact interactions, and hydrogen bonding in detail. In the MM-GBSA approach, binding free energy is calculated using the summation of three main components surface area term hydrophobic effects are mostly represented by this. Implicit solvation is taken into consideration by generalised born solvation energy. Van der waals and electrostatic interactions are captured by molecular mechanics energy. The free energy of each protein and ligand will be deducted from the total free energy of the protein–ligand complex in order to estimate the binding energy [14]. This computation will provide important information regarding the strength and stability of the ligand-target interaction. In addition, the MM-GBSA technique incorporates physics-based adjustments to handle interaction effects not represented by traditional energy terms. The dependability of binding affinity predictions will rise as a result of these improvements, enabling more accurate assessment of ligand-protein interactions.

Calculations of ADME

It was predicted that the pharmacokinetic characteristics for the protein-ligand complexes, namely ADME, would be determined using Schrödinger Suite 2023-4. When needed, homology modelling was used homology modelling to construct protein structures, or experimentally resolved data. Ligand molecules were created using typical molecular modelling procedures. The QikProp module included in Schrödinger's Prime program was utilised for ADME prediction [15]. The OPLS3-2005 force field was used to precisely simulate molecular interactions. It is a revised version of the optimised potentials for liquid simulations (OPLS3) force field and is well known for its improved ability to predict molecular characteristics and protein–ligand behaviour. The VSGB 2.0 (variable solvent generalised born) solvation model was used to mimic the solvation environment by taking into account the dynamic character of the solvents in biological systems. Proteins and ligands were pre-processed utilising Schrödinger preparation techniques, which also included energy minimisation towards physiological pH and the assignment of suitable protonation states. Next OPLS3-2005 force field was used to further minimise protein–ligand interactions in order to get low-energy conformations. Finally, ADME characteristics such as oral absorption, excretion, metabolism, and permeability using QikProp [16]. This will provide us with trustworthy estimates derived from empirical models that have been verified.

RESULTS

Molecular docking results and analysis

Using the Papain-like protease (PLpro) crystal structure Schrödinger Suite 2023-4 was used to conduct molecular docking investigations. By using a virtual screening technique, the root mean square deviation (RMSD) of ligand conformations was guaranteed to be less than 1.5 Å when compared to the co-crystallised structure. Lipinski's rule of five was used to exclude functional groups that had negative impacts on interactions between ligands and proteins. When assessing docking outcomes, Glide XP-docking settings were taken into account. This is significant since it contains the glide score, e-model, van der Waals energy (E_{vdw}), coulomb energy (E_{coul}) and total docking energy (E_{energy}). The docked ligands binding orientation, interaction strength, and binding efficiency were rigorously examined based on these factors table 1.

Table 1: The XP-docking scores for compounds 1-10 in the (PLpro) catalytic pocket (PDB ID: 7D4F)

Compound	Glide score (kcal/mol)	Glide van der waals (kcal/mol)	Glide coulomb (kcal/mol)	Glide energy (kcal/mol)	Glide E-model
1	-3.81	-30.86	-7.17	-38.04	-51.95
2	-5.31	-26.79	-13.33	-40.12	-54.07
3	-4.05	-29.80	-11.75	-41.56	-56.07
4	-3.85	-32.86	-11.82	-44.09	-56.55
5	-2.63	-30.30	-11.57	-41.87	-54.95
6	-4.13	-34.84	-10.21	-45.05	-62.19
7	-3.11	-30.41	-11.86	-42.28	-54.40
8	-3.51	-32.94	-8.04	-40.48	-51.38
9	-3.71	-28.94	-8.36	-37.30	-49.66
10	-2.46	-31.69	-11.75	-43.44	-59.37
Co-crystal	-2.10	-23.73	-1.09	-24.67	-30.88

Glide Score = overall docking score; van der Waals = steric/hydrophobic interactions; Coulomb = electrostatic interactions; Glide Energy = sum of van der Waals and Coulomb energies; E-model = docking pose ranking score. More negative values indicate stronger binding affinity. (Docking calculations were performed using Glide (Schrödinger Suite 2023-4) in Extra Precision (XP) mode).

All of the compounds exhibited favourable binding activity, according to the docking study results, able it a small number of compounds outperformed the conventional medication co-crystal ligand in terms of efficacy. Significantly, compounds 2, 3, and 6 had the greatest glide scores-5.31 kcal/mol,-4.05 kcal/mol, and-4.13 kcal/mol, respectively which show strong binding affinity. Despite having more negative glide scores (–3.85, –3.11, –3.51 kcal/mol, and –3.71 kcal/mol), compounds 4, 7, 8, and 9 also demonstrated strong binding potential. However, compounds 5 and 10, with glide scores of –2.63 kcal/mol and –2.46 kcal/mol, respectively, demonstrated weaker binding interactions. The scores for the standard co-crystal ligand glide were-2.10 kcal/mol, respectively, which were significantly more negative than those of the compounds under examination. Compound 2 in particular displayed the strongest interaction characteristics of all the chemicals. Van der waals energy (E_vdw) = –26.79 kcal/mol, Coulomb energy (E_coul) = –13.33 kcal/mol, total docking energy (E_energy) = –40.12 kcal/mol, and e-model (G_emodel) score = –54.07 kcal/mol were found in this.

Table 2: Binding free energy (MM-GBSA) contribution (kcal/mol) for compounds 1–10in the (PLpro) complexes

Compound	ΔG_{bind}(kcal/mol)	Coulomb energy (kcal/mol)	H-bond energy (kcal/mol)	Lipophilic energy (kcal/mol)	Generalized energy	van der waals (kcal/mol)
1	-44.26	-50.31	-1.22	-18.80	2.92	-41.21
2	-74.24	-53.10	-1.67	-18.56	2.68	-40.28
3	-42.21	-53.16	-1.39	-16.62	2.26	-40.75
4	-35.29	-38.74	-2.19	-16.42	1.54	-34.99
5	-50.92	-41.23	-1.97	-13.34	4.12	-36.55
6	-72.39	-60.70	-2.09	-21.15	3.67	-46.16
7	-60.73	-59.09	-2.30	-18.82	2.32	-36.28
8	-44.70	-45.32	-1.62	-16.11	2.75	-33.88
9	-54.68	-47.66	-1.82	-21.10	2.23	-34.61
10	-52.33	-37.35	-1.71	-16.13	2.86	-36.37
Co-crystal	-54.50	-58.66	-2.12	-17.57	2.42	-37.91

ΔG_{bind}= binding free energy calculated without inclusion of the entropy (−TΔS) contribution; (more negative indicates stronger enthalpy-driven binding); Coulomb = electrostatic interactions; H-bond = hydrogen bonding contribution; Lipophilic = hydrophobic interactions; van der Waals = steric contribution.

Comparing all the results table 2 compound 2 emerges as the most promising compound showing comparable or even superior binding affinity on papain-like protease (PLpro) when compared with the co-crystal ligand. Because of this, it is identified as a strong lead candidate for further in-depth computational and experimental studies. Compound 2 had a binding free energy of-74.24 kcal/mol. The major contributions of hydrophobic energy (Lipo –18.56 kcal/mol), van der waals energy (–40.28 kcal/mol), and coulombic energy (–53.10 kcal/mol) are responsible for this favourable binding. Combining all of this makes compound 2's great binding potential very evident. In the same way, compound 6 had a similar binding free energy of-72.39 kcal/mol. Notably, the hydrophobic contribution (–21.15 kcal/mol) and van der waals energy (–46.16 kcal/mol) were relatively smaller, but the coulombic energy contribution was greater (–60.70 kcal/mol). Co-crystal ligand demonstrated more negative binding free energy of-54.50 kcal/mol, respectively. Out of all the chemicals examined, only compound 2 had the highest binding affinity. It should be noted that the MM-GBSA ΔGbind values may be overestimated due to exclusion of the entropy term (−TΔS); therefore, these energies are interpreted only for relative ranking of compounds rather than absolute binding affinity. Its promise has been strengthened by its designation as a promising candidate for more in-depth research, since it demonstrated equivalent or even better performance than a co-crystal ligand.

Hydrogen bonding and amino acid interactions

The hydrogen bond interactions between each molecule and the amino acid residues found in the catalytic pocket of papain-like protease (PLpro) (PDB ID: 7D4F) were thoroughly discussed in fig. 3. The stability and binding affinity of the protein-ligand complexes are significantly influenced by these hydrogen bonding interactions. In addition to having a substantial impact on overall molecular interactions, this will also have a considerable impact on the compounds' potential inhibitory efficacy.

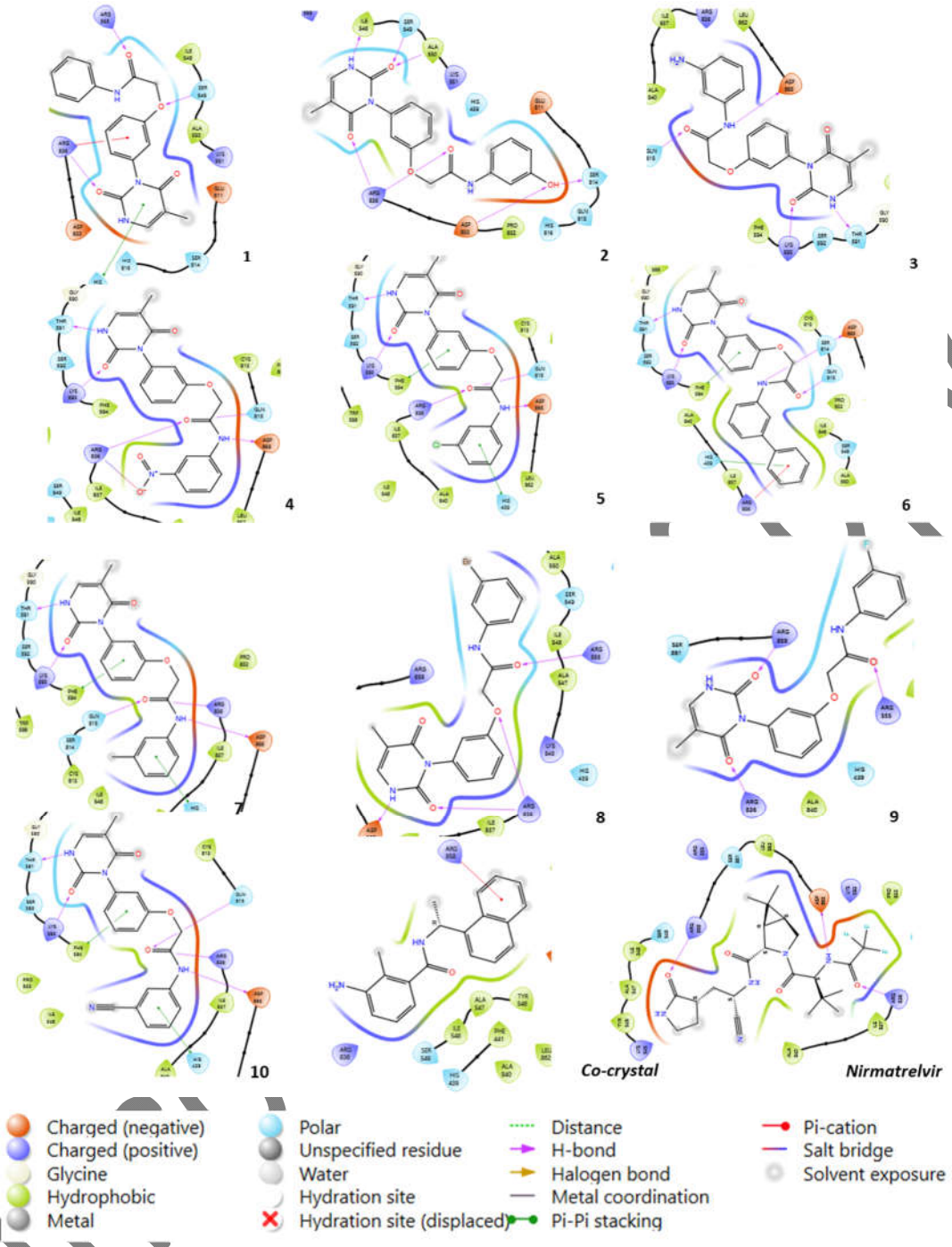

Fig. 3: Compounds 2D Interaction diagrams in the PLprocatalytic pocket 1-10 with Co-crystal (The diagrams illustrate key molecular interactions, including hydrogen bonds, hydrophobic contacts, and π–π or π–cation interactions formed between the ligands and catalytic site residues)

Ligand–protein interaction analysis

The hydrogen bond interactions between the designed ligands and the active site residues of *SARS-CoV-2* papain-like protease ((PLpro), PDB ID: 7D4F) are summarized in table 4. Most ligands displayed favorable hydrogen bonding within the catalytic pocket, supporting their potential inhibitory activity. Compound 2 established seven hydrogen bonds within the PLpro active site, primarily mediated through its carbonyl (C=O), hydroxyl (–OH), and amine (–NH) functional groups. The carbonyl oxygen acted as a hydrogen bond acceptor with the backbone NH of Ile548 and Ala550, while the hydroxyl group formed hydrogen bond donor interactions with Ser549 and Ser814. In addition, the amine moiety participated as a hydrogen bond donor toward Asp833 and Arg836. These residues (Ile548, Ser549, Ala550, Asp833, Arg836, and Ser814) serve as key anchoring residues, collectively stabilizing Compound 2 within the catalytic pocket and contributing significantly to its enhanced binding affinity.

Compounds 4, 5, 7, and 10 also formed multiple hydrogen bonds (five each) with residues such as Lys593, Thr591, Arg836, Asp865, and Gln815, further supporting their high binding affinity. Frequent interactions were observed with critical residues, including Lys593, Arg836, Asp865, Thr591 and Gln815, which play a significant role in substrate recognition and catalysis of (PLpro). These residues were consistently targeted by the

designed ligands, suggesting that they contribute substantially to ligand anchoring and inhibitory potential. *Nirmatrelvir* is shown only for contrast and was not considered as a PLpro docking control. Overall, the interaction profiles confirm that the designed compounds effectively engage key catalytic and structural residues of (PLpro), thereby reinforcing their therapeutic potential against COVID-19.

Table 4: Hydrogen bond interactions between designed ligands and active site residues of (PL^{pro}) (PDB ID: 7D4F)

Compound	No. of H-bonds	Interacting residues	Type of interaction
1	3	Arg555, Arg836, Ser549	C=O, O hydrogen bond
2	7	Ile548,Ser549,Ala550,Arg836,Asp833,Ser814	C=O,OH,NH hydrogen bond
3	4	Gln815,Asp865,Lys593,Thr591	NH, C=O hydrogen bond
4	5	Lys593, Thr591,Arg836,Asp865,Gln815	NH and C=O hydrogen bonds
5	5	Thr891,Lys593,Arg836,Glu815,Asp865	NH and C=O hydrogen bonds
6	4	Thr891,Lys593,Asp865,Gln815	NH and C=O hydrogen bonds
7	5	Thr891,Lys593,Gln815,Asp865,Arg836	NH and C=O hydrogen bonds
8	3	Arg555,Arg836,Asp865	NH,O,C=O hydrogen bond
9	3	Arg555,Arg333,Arg836	C=O hydrogen bond
10	5	Thr591,Lys593,Gln313,Arg836,Asp363	C=O and NH hydrogen bonds
Co-crystal	-	-	-

H-bond interactions were identified from 2D interaction diagrams generated using Schrödinger Maestro. Key residues such as Lys593, Thr591, Arg836, Asp865, and Gln815 were consistently involved in ligand anchoring, confirming their crucial role in stabilizing the ligands within the PLpro active site of SARS-CoV-2.

ADME study results

The assessed the pharmacokinetic behaviour and safety profiles of the drugs included in this study after examining the ADME characteristics of the ten compounds. Although table 4 summarises the data, a thorough explanation of their interpretation is provided here.

Table 4: ADME Properties of compounds 1-10

Compound	CNS activity	SASA (Å^2)	H-bond donors	H-bond acceptors	logP_{o/w}	logHERG	Caco-2 permeability	logBBB	Human oral absorption (%)	PSA (Å^2)	Rule of five violations
1	-2	652.21	2	6	2.70	-4.41	287.81	-1.37	3	114.05	0
2	-2	672.43	3	7	1.95	-4.04	286.96	-2.05	3	136.77	0
3	-2	674.26	3	7	1.79	-4.03	274.63	-2.13	3	140.52	0
4	-2	698.19	2	7	2.01	-4.35	234.07	-2.57	2	159.18	0
5	-2	680.47	2	6	3.18	-4.32	284.86	-1.24	3	114.15	0
6	-2	772.84	2	6	3.67	-5.55	308.44	-1.54	1	113.63	0
7	-2	691.43	2	6	3.02	-4.13	289.48	-1.43	3	114.20	0
8	-2	685.26	2	6	2.26	-4.13	285.99	-1.23	3	114.12	0
9	-2	667.24	2	6	2.94	-4.38	291.11	-1.28	3	113.65	0
10	-2	696.69	2	6	1.98	-4.26	259.54	-2.30	2	139.98	0
Co-crystal	-2	620.13	2	6	2.27	-4.56	267.89	-2.15	3	127.09	0

CNS = central nervous system activity (−2 inactive to+2 active); SASA = solvent accessible surface area (300–1000 Å^2); logP_{o/w}= octanol/water partition coefficient (<5); logHERG = prediction of hERG inhibition (>−5 (lower = cardiotoxic risk); Caco-2 = intestinal permeability (>500 nm/s (high),<25 nm/s (low); logBBB = blood–brain barrier penetration (−1.0 to+0.5); PSA = polar surface area (<140 Å^2); Rule of Five = Lipinski compliance (≤1 violation acceptable).

ADME analysis indicated that all ten compounds exhibited very low predicted central nervous system (CNS) penetration, with CNS scores of −2. This score reflects limited blood–brain barrier permeability and suggests that the compounds are likely to act peripherally, which may be advantageous in minimizing potential CNS-related off-target effects rather than implying a complete absence of CNS side effects. The low predicted BBB penetration may help minimize CNS-related off-target effects; however, it does not completely rule out potential CNS involvement. The values of solvent accessible surface area (SASA) ranged from 652.21Å^2 to 772.84Å^2. Favourable surface interactions and efficient absorption potential are reflected in this. These compounds have two to three hydrogen bond donors and six to seven hydrogen bond acceptors, which provide information on the ideal hydrogen bonding capacity required for target engagement. It is clear that there is a good balance between membrane permeability and water solubility since lipophilicity (QPlogP) values ranged from 1.79 to 3.67. Likewise, the range of Caco-2 permeability values was 234.07 to 308.44 nm/s. It is reasonable to assume that these chemicals may have improved intestinal absorption due to the greater levels. (No artificial intelligence (AI)–based tools were used at any stage of this study. All compound design, molecular docking, MM-GBSA calculations, ADMET predictions, and fig. preparation were performed using established, traditional molecular modeling and cheminformatics software only.)

DISCUSSION

Up to now, natural substances, repurposed medications, and artificial scaffolds have all been assessed potential *SARS COV-2* protein inhibitors in several computational and experimental investigations. The inhibitory action of *phycobilins*, *phytochemicals*, and food-derived bioactive on Mpro and PLpro has been shown in earlier investigations. Its docking scores were between-9.8 and-7.6kcal/mol [17]. *Amentoflavone*, *gallocatechin gallate, theaflavin-3*, and *3-digallate* are examples of plant-derived chemicals that have demonstrated successful binding with PLpro. Simulations using molecular dynamics further verified the stability of these compounds [18]. Our *pyrimidine-based* compounds have more negative docking scores when was compare all of these. Compounds 2 and 6 are-5.31 and-4.13kcal/mol, respectively. However, the most important thing to take into

account is that the compounds Asp164 and Gln269, which are the catalytic residues of PLpro, have demonstrated strong hydrogen bonding. This form of interaction will resemble the binding mode seen in crystallographic ally verified inhibitors such as GRL-0617. This structural mimicry aligns with the earlier PLpro structural investigations. These investigations have demonstrated the significance of substrate recognition sites (S3/S4 and Sub2) for ligand binding [19]. The conformational entropy term (−TΔS) was not included in the MM-GBSA binding free energy calculations due to the high computational cost associated with normal mode analysis. Therefore, the reported ΔG_bind values represent enthalpy-dominated estimates and may overestimate the actual binding affinity. Also discovered that the stated MM-GBSA binding free energy for previous hit compounds ranged from-15.8 to-36.6 kcal/mol. However, found extremely high negative MM-GBSA binding free energy values for our compounds, such as Compound 2 =-74.24 kcal/mol and Compound 6 =-72.39 kcal/mol. More binding affinity and improved thermodynamic stability are indicated by this. This is also in line with current flexible docking and interaction finger-based computational techniques that have shown a high biological activity connection with PLpro inhibitors [20]. Prior repurposed antiviral medications, such as *lopinavir* and *ritonavir*, have issues with low oral absorption and bioavailability when viewed from a pharmacokinetic standpoint. Our developed *pyrimidine* compounds, on the other hand, adhere to Lipinski's rule of five, exhibit good intestinal permeability, and have minimal CNS penetration, all of which contribute to their superior drug like profile. This overcomes the known limits of previous repurposed antivirals and promotes broad-spectrum antiviral scaffolds, which are essential for addressing issues like viral mutations. Nevertheless, the relative ranking remains meaningful and consistently indicates stronger predicted binding for Compounds 2 and 6 compared with the other evaluated compounds. These results are comparable to those of previously reported PLpro inhibitors such as *GRL0617*. In particular, *GRL0617* has been reported to exhibit key interactions with the Tyr268 region within the substrate-binding pocket of PLpro. Similarly, the present *pyrimidine-based* compound demonstrates stable interactions with the same critical region, suggesting that it represents a structurally viable alternative to established PLpro inhibitors [21]. Our *pyrimidine-based* derivatives are either equivalent or exhibit greater performance in docking, binding affinity, and ADMET parameters when compared to natural molecules, repurposed medicines, and synthetic scaffolds. Since the entropy contribution (−TΔS) was not included in MM-GBSA calculations, the absolute ΔGbind values are likely overestimated. Hence, the present analysis focuses on comparative binding trends and relative ranking of the designed compounds rather than their absolute binding strengths. Because of this, these findings establish *pyrimidine* scaffolds as viable lead options for the development of PLpro-targeted *SARS-CoV-2* antivirals.

CONCLUSION

In this study, novel *pyrimidine-based* compounds targeting the papain-like protease (PLpro) of *SARS-CoV-2* using an *in silico* approach. Molecular docking, MM-GBSA binding free energy calculations, and ADMET profiling indicated that compounds 2 and 6 exhibit favourable (more negative) binding energies, predicted *thermodynamic* stability, and acceptable pharmacokinetic properties when compared with the co-crystallised reference ligand. The proposed ligands formed key hydrogen bond interactions with essential catalytic residues of PLpro, supporting their potential binding relevance. Although these findings are derived from computational analyses and should be interpreted cautiously, they highlight the *pyrimidine* scaffold, particularly compound 2, as a promising candidate for further experimental validation through *in vitro* enzymatic inhibition assays and antiviral activity studies.

ACKNOWLEDGMENT

The authors would like to thank the Department of Pharmaceutical Chemistry, Arulmigu Kalasalingam College of Pharmacy, Krishnan Koil, and Department of Pharmaceutics, Sri Balaji Vidyapeeth School of pharmacy, Karaikal, Pondicherry, for providing facilities for conducting Research.

FUNDING

No funding was received for this work.

AUTHORS CONTRIBUTIONS

Habeeb Raja S, Anbu Murugan S P, Irfana k-Conceptualization, validation, and data curation. Susmitha V, Arun Kesavh S, Nitheesh A-Data curation, methodology, and writing review and editing. Muthukumaran M, Mohd Abdul Baqi-original draft preparation, Conceptualization, validation and data curation.

CONFLICT OF INTERESTS

Declared none

REFERENCES

1. To KK, Sridhar S, Chiu KH, Hung DL, Li X, Hung IF et al. Lessons learned 1 year after *SARS-CoV-2* emergence leading to *COVID-19* pandemic. Emerg Microbes Infect. 2021 Jan;10(1):507-35. doi: 10.1080/22221751.2021.1898291, PMID 33666147.
2. Chauhan S. Comprehensive review of coronavirus disease 2019 (*COVID-19*). Biomed J. 2020;43(4):334-40. doi: 10.1016/j.bj.2020.05.023, PMID 32788071. bj.2020.05.023.
3. Gorkhali R, Koirala P, Rijal S, Mainali A, Baral A, Bhattarai HK. Structure and function of major *SARS-CoV-2* and *SARS-CoV proteins*. Bioinform Biol Insights. 2021 Jan;15:11779322211025876. doi: 10.1177/11779322211025876, PMID 34220199.
4. Zhang Q, Jia Q, Gao W, Zhang W. The role of *deubiquitinases* in virus replication and host innate immune response. Front Microbiol. 2022;13:839624. doi: 10.3389/fmicb.2022.839624, PMID 35283827.
5. Lai CM, Chen WJ, Qin Y, Xu D, Lai YK, He SH. Innovative hydrogel design: tailoring immunomodulation for optimal chronic wound recovery. Adv Sci (Weinh). 2025 Jan;12(2):e2412360. doi: 10.1002/advs.202412360, PMID 39575827.
6. Yin W, Luan X, Li Z, Zhou Z, Wang Q, Gao M et al. Structural basis for inhibition of the *SARS-CoV-2 RNA polymerase by suramin*. Nat Struct Mol Biol. 2021;28(3):319-25. doi: 10.1038/s41594-021-00570-0, PMID 33674802.
7. Suryawanshi SS, Jayannache PB, Patil RS. Ms P, sg A. Molecular docking studies on screening and assessment of selected *bioflavonoids* as potential inhibitors of *COVID-19* main protease. Asian J Pharm Clin Res. 2020;13(9):174-8. DOI. doi: 10.22159/ajpcr.2020. v13i9.38485.
8. Ibrahim TM, Ismail MI, Bauer MR, Bekhit AA, Boeckler FM. Supporting *SARS-CoV-2* papain-like protease drug discovery: *in silico* methods and benchmarking. Front Chem. 2020;8:592289. doi: 10.3389/fchem.2020.592289, PMID 33251185.
9. Indhumathi s, Nithi SS, Gobiananth, Baqi MA, Venkatheshan N, Meena G et al. Design and *in silico* evaluation of *phenoxy acetamide* derivatives as potential antidiabetic agents. Int J App Pharm. 2025;17(5):159-67. doi: 10.22159/ijap.2025v17i5.54892.
10. Imam SS, Imam ST, Mdwasifathar K, Kumar R, Ammar MY. Interaction between ace 2 and *SARS-CoV-2*, and use of EgcgAnd*Theaflavin* to treat *Covid 19*. Int J Curr Pharm Sci. 2022;14:5-10. doi: 10.22159/ijcpr.2022v14i2.1945.
11. Badavath VN, Sinha BN, Jayaprakash V. Design, *in silico* docking and predictive ADME properties of novel *pyrazoline* derivatives with selective human MAO inhibitory activity. Int J Pharm Pharm Sci. 2015;7:277-82.

12. Azam F, Eid EE, Almutairi A. Targeting *SARS-CoV-2 m*ain protease by *teicoplanin*: A mechanistic insight by docking, MM/GBSA and molecular dynamics simulation. J Mol Struct. 2021;1246:131124. doi: 10.1016/j.molstruc.2021.131124. PMID 34305175.
13. Sgobba M, Caporuscio F, Anighoro A, Portioli C, Rastelli G. Application of a post-docking procedure based on MM-PBSA and MM-GBSA on single and multiple protein conformations. Eur J Med Chem. 2012;58:431-40. doi: 10.1016/j.ejmech.2012.10.024, PMID 23153814. ejmech.2012.10.024.
14. Parveen S, Khalil R, Shafiq N, Rashid M, Nazli Z i H, Dawoud TM, Metouekel A, Bourhia M, Younous YA, Moveed A. Therapeutic switching of *metronidazole* anti-cancerous compounds as anti *SARS-COV-2* inhibitors: integration of QSAR, molecular docking, MD simulation and ADMET analysis. *Discov Life.* 2024 Aug 9;54(1):10. DOI: https://doi. org/10.1007/s11084-024-09653-6.
15. Dash S, Rathi E, Kumar A, Chawla K, Kini SG. Identification of DprE1 inhibitors for tuberculosis through integrated in-silico approaches. Sci Rep. 2024;14(1):11315. doi: 10.1038/s41598-024-61901-x, PMID 38760437.
16. Wu C, Liu Y, Yang Y, Zhang P, Zhong W, Wang Y et al. Analysis of therapeutic targets for *SARS-CoV-2* and discovery of potential drugs by computational methods. Acta Pharm Sin B. 2020;10(5):766-88. doi: 10.1016/j.apsb.2020.02.008. PMID 32292689.
17. Swargiary A, Mahmud S, Saleh MdA. Screening of phytochemicals as potent inhibitor of *3-chymotrypsin* and papain-like proteases of *SARS-CoV2*: an *in silico* approach to combat *COVID-19*. J Biomol Struct Dyn. 2022 Mar 24;40(5):2067-81. doi: 10.1080/07391102.2020.1835729, PMID 33089730.
18. Valdés-Albuernes JL, Díaz-Pico E, Alfaro S, Caballero J. Modeling of *noncovalent* inhibitors of the papain-like protease (PLpro) from *SARS-CoV-2* considering the protein flexibility by using molecular dynamics and cross-docking. Front Mol Biosci. 2024;11:1374364. doi: 10.3389/fmolb.2024.1374364, PMID 38601323.
19. Varghese A, Liu J, Liu B, Guo W, Dong F, Patterson TA et al. Analysis of structures of *SARS-CoV-2* papain-like protease bound with ligands unveils structural features for inhibiting the enzyme. Molecules. 2025;30(3):491. doi: 10.3390/molecules30030491, PMID 39942596.
20. Pendyala B, Patras A, Dash C. *Phycobilins* as potent food bioactive broad-spectrum inhibitors against proteases of *SARS-CoV-2* and other *coronaviruses*: A preliminary study. Front Microbiol. 2021;12:645713. doi: 10.3389/fmicb.2021.645713, PMID 34177827.
21. Ratia K, Pegan S, Takayama J, Sleeman K, Coughlin M, Baliji S et al. A *noncovalent* class of papain-like protease/*deubiquitinase* inhibitors blocks *SARS* virus replication. Proc Natl Acad Sci U S A. 2008 Oct 21;105(42):16119-24. doi: 10.1073/pnas.0805240105, PMID 18852458.